Published in final edited form as:
J Mol Biol. 2007 February 16; 366(2): 574–585.

Point mutations in the HIV-1 matrix protein turn off the myristyl switch

Jamil S. Saad[1], **Erin Loeliger**[1], **Paz Luncsford**[1], **Mellisa Liriano**[1], **Janet Tai**[1], **Andrew Kim**[1], **Jaime Miller**[1], **Anjali Joshi**[2], **Eric O. Freed**[2], and **Michael F. Summers**[1,*]

1 *Howard Hughes Medical Institute and Department of Chemistry and Biochemistry, University of Maryland Baltimore County, 1000 Hilltop Circle, Baltimore, Maryland 21250 USA*

2 *Virus-Cell Interaction Section, HIV Drug Resistance Program, National Cancer Institute, Frederick, MD 21702-1201*

Abstract

During the late phase of HIV-1 replication, newly synthesized retroviral Gag proteins are targeted to lipid raft regions of specific cellular membranes, where they assemble and bud to form new virus particles. Gag binds preferentially to the plasma membrane (PM) of most hematopoietic cell types, a process mediated by interactions between the cellular PM marker phosphatidylinositol-(4,5)-bisphosphate ($PI(4,5)P_2$) and Gag's N-terminally-myristoylated matrix (MA) domain. We recently demonstrated that $PI(4,5)P_2$ binds to a conserved cleft on MA and promotes myristate exposure, suggesting a role as both a direct membrane anchor and myristyl switch trigger. Here we show that $PI(4,5)P_2$ is also capable of binding to MA proteins containing point mutations that inhibit membrane binding *in vitro*, and *in vivo*, including V7R, L8A and L8I. However, these mutants do not exhibit $PI(4,5)P_2$- or concentration-dependent myristate exposure. NMR studies of V7R and L8A MA reveal minor structural changes that appear to be responsible for stabilizing the myristate-sequestered (myr (s)) species and inhibiting exposure. Unexpectedly, the myristyl group of a revertant mutant with normal PM targeting properties (V7R,L21K) is also tightly sequestered and insensitive to $PI(4,5)P_2$ binding. This mutant binds $PI(4,5)P_2$ with two-fold higher affinity compared with the native protein, suggesting a potential compensatory mechanism for membrane binding.

Keywords

Human immunodeficiency virus type-1 (HIV-1); Gag; myristyl (myr); matrix (MA); phosphatidylinositol-4,5-bisphosphate ($PI(4,5)P_2$); analytical ultracentrifugation (AU); nuclear magnetic resonance (NMR)

Introduction

The assembly of retroviruses in infected cells proceeds by complex, multi-stepped mechanisms that are only beginning to become understood. The major structural constituent of retroviruses is called Gag, a multi-domain protein that is post-translationally acylated (acetylated in the alpharetroviruses and myristoylated in most other retroviruses). Several thousand copies of Gag assemble to form a single virus particle, which is enveloped by a lipid bilayer derived

* Corresponding author: Phone: (410)-455-2527; FAX: (410)-455-1174; Email: summers@hhmi.umbc.edu.

from the host cell. Although the Gag proteins of the betaretroviruses assemble in the cytoplasm prior to budding from the plasma membrane[1], the Gag proteins of most other retroviruses (including the human immunodeficiency virus type-1, HIV-1) assemble at cellular membranes and require the assistance of host factors associated with the endosomal protein sorting machinery[2,3]. In most hematopoetic cell types, the HIV-1 Gag proteins assemble and bud from the plasma membrane (PM)[4,5]. Some studies suggest that assembly in macrophages occurs mainly at the membranes of late endosomes and/or multivesicular bodies (MVBs)[6–8], although the significance of endosomal assembly has recently been questioned[9]. The Gag proteins co-localize at punctate sites[10,11], and analysis of the lipid and lipid-bound protein components of isolated virions indicates that the viral membranes are derived from lipid raft microdomains. Lipid rafts are enriched with cholesterol and sphingolipids with saturated fatty acid chains, and form liquid-ordered membrane structures that serve as preferential binding sites for specific cellular proteins. Several animal viruses are known to associate with rafts upon cellular entry and/or egress[11].

The trafficking of Gag to membrane assembly sites is mediated by the protein's N-terminal matrix (MA) domain. Tight binding of the HIV-1 Gag protein to the PM is driven by a bipartite signal that constitutes a myristyl group (myr) and a cluster of basic residues on the surface of the MA protein [12,13]. Mutations and/or deletions within the first 6 residues (Gly-2 to Ser-6; myristate group is residue number 1) of MA that affect Gag myristylation [14–18], or within the polybasic region of MA [5,12,19,20], impair membrane binding *in vitro* and can retarget Gag to the cytoplasm and/or intracellular compartments *in vivo*. In addition, there is considerable evidence that the affinity of MA binding for membranes is significantly lower than that of the intact Gag molecules, which led to the suggestion that Gag binding may be mediated by a myristyl switch mechanism.[21,22] In addition to promoting membrane binding, myristate exposure appears to be required for targeting Gag to lipid rafts. Resh and co-workers showed that substitution of the saturated myristyl group of HIV-1 Gag by unsaturated lipids reduces the affinity of Gag for rafts, but not for membranes in general, leading to particle assembly defect.[23]

Mutagenesis studies have identified residues in the N-terminus of HIV-1 MA that are critical for proper membrane selection, including point mutations such as V7R, L8A and L8I. [19,24–26] These substitutions give rise to a phenotype similar to that observed for the unmyristoylated protein, although they do not block myristoylation. They severely inhibit virus assembly and release, cause significant reductions in PM binding, and lead to significant increases in cytosolic localization of Gag. [19,24–26] Interestingly, the assembly-defective phenotype imposed by the V7R mutation is reversed by second-site compensatory mutations elsewhere in the MA domain. Biochemical studies have shown that L21K and K98E mutations reversed the membrane-binding defect caused by V7R and significantly increased Gag binding to the PM. [24] These findings suggested that mutations at positions 7 and 8 may block myristate exposure, and that compensatory substitutions at positions 21 and 98 might restore exposure.

NMR studies confirmed that the HIV-1 MA myristyl group is capable of adopting sequestered (myr(s)) and exposed (myr(e)) conformations, and demonstrated that myristate exposure can be promoted by factors that increase protein self-association[27]. More recently, the myristyl switch equilibrium was shown to be sensitive to binding by phosphatidyl-4,5-bisphosphate (PI(4,5)P_2), a cellular factor that serves as a membrane marker for proteins that need to associate specifically with the plasma membrane[28–31]. PI(4,5)P_2 plays a major role in directing HIV-1 Gag to the PM[32], and appears to function by acting as both a trigger for myristate exposure and as a direct membrane anchor[31]. To determine the mechanism(s) by which the position-7 and –8 mutations affect *in vivo* Gag localization and virus assembly, we conducted NMR and thermodynamic studies on the HIV-1 MA mutants V7R, L8A, L8I, L21K, and V7R/L21K (Figure 1), and studied interactions between these mutants and PI(4,5)P_2. Our findings reveal

that the single-residue mutations do not inhibit PI(4,5)P_2 binding, but do inhibit PI(4,5)P_2- and concentration-dependent myristate exposure and suggest a novel potential compensatory mechanism for membrane selection and binding by the V7R/L21K revertant mutant.

Results

V7R, L8A and L8I point mutations inhibit myristate exposure and protein self-association

Single point mutations in the HIV-1 MA protein (V7R, L8A and L8I) were made by site-directed mutagenesis of a co-expression vector harboring the yeast N-terminal myristyl transferase (yNMT) and HIV-1 MA gene. [27] These substitutions did not adversely affect myristylation efficiencies (~100%, compared to ~90/10% myr/myr(-) for the wild-type MA protein; Mmeas:Mcalc = 15801.4:15801.7, 15701.9:15702.5, and 15744.9:15744.6 for V7R, L8A and L8I MA, respectively). ^{1}H and ^{15}N NMR signals observed in two dimensional (2D) [^{1}H–^{15}N] HSQC spectra obtained for V7R, L8A and L8I were insensitive to concentration over the range of 50 μM to 0.9 mM (Figure 1). In contrast, for the wild type (WT) myrMA protein, a subset of signals shift progressively toward the frequencies observed for myr(-)MA upon increasing the protein concentration due to a concomitant shift in the monomer-trimer equilibrium toward the trimeric species and exposure of the myristyl group.[27] The absence of concentration-dependent shifts for V7R, L8A, and L8I indicates that these mutants exist in a unique conformation over the range of concentrations tested. Sedimentation equilibrium (SE) data obtained for V7R, L8A and L8I are similar in appearance to SE data obtained for myr(-) MA, and confirm that the myrMA mutants remain monomeric at concentrations as high as 1 mM.

NMR analysis of V7R-, L8A- and L8I-myrMA

To elucidate the conformational changes that occur upon substituting a single amino acid in the N-terminus of myrMA, a combination of ^{15}N-, ^{13}C-, ^{15}N/^{13}C-, ^{13}C/^{13}C- and ^{13}C-edited/^{12}C-double-half-filtered NOE experiments were collected for V7R, L8A, and L8I proteins. In all spectra obtained for the three mutants, minor changes were observed in the pattern of NMR shifts and intensities for residues located in close proximity to the mutation site (Ser-6 – Gly-10). For residues 11–132, no new intraprotein NOEs were detected that would be indicative of an altered protein conformation. Representative portions of the 4D ^{15}N,^{13}C-edietd NOE data obtained for V7R are presented in Figure 2. NOE cross-peaks between protein residues and myristate group are not observed in this dataset because the myristate group is not ^{13}C-labeled. However, 2D NOESY, 3D ^{13}C-edited NOE, and 3D ^{13}C-edited/^{12}C-double-half-filtered NOE data obtained for V7R, L8A, and L8I show numerous unambiguous NOEs between the myristate group and the side chains of Val-/Arg-7, Leu-/Ala-/Ile-8, Trp-16, ILe-34, Val-35, Ser-38, Gly-49, Leu-51, Glu-52, and Leu-85 (Figure 2 and 3). For V7R, NOEs between the myristate group and both Arg-7 (Hβ2/3, Hγ2/3, and Hδ2/3) and Leu-8 (Hβ2/3, Hγ, and Hδ1/2) side chains are clearly observed in the 3D ^{13}C-edited/^{12}C-double-half-filtered NOE data (Figure 2), indicating that the myristate group is sequestered and that the side chains of Arg-7 and Leu-8 are packed against the myristate group. Similar NOEs between the myristate group and side chains of Val-7 and Ala/Ile-8 were also observed for L8A and L8I (Figure 3). NOEs between the myristate group and the side chains of Val-7 and Leu-8 were also observed for the WT myrMA protein. [27] These NMR observations indicate that mutation of Arg-7 and Leu-8 does not greatly alter the conformation of the loop and that residues 7 and 8 play an important role into the stabilization of the myr(s) form.

For V7R and L8I, the terminal methyl group (myr-C^{14}H$_3$) exhibited an upfield chemical shift comparable to that observed for the WT myrMA protein (~0.5 ppm). [27] Structural analysis of the WT myrMA protein revealed that the terminal myr-C^{14}H$_3$ group packs against the side

chain of Trp-16. For L8A, the myr-$C^{14}H_3$ group exhibited a larger upfield shift (~0.3 ppm), indicating that the methyl group is packed even closer to the aromatic ring of Trp-16.

Structures of V7R- and L8A-myrMA

We chose V7R and L8A proteins as representative models to study the structural changes that led to the stabilization of myristyl-sequestered form. Superpositions of 20 structures for V7R and L8A generated from NMR data (500–800 μM and 35°C) are shown in Figure 4. The backbone atoms of Val-7–Ile-104 are well defined and are very similar to the coordinates of the WT myrMA protein (Figure 5 and Table 1),[27,31] indicating that single mutations in the N-terminal loop had no effect on the globular fold of the protein. The myristyl group adopts an extended conformation with the myr-$C^{14}H_3$ group packing in close proximity to the side chains of core residues Trp-16, Ile-34, and Leu-85, and other myristate methylene groups interacting with the side chains of Ala-5, Ser-6, Val-7, Ile-34, Ser-38, Pro-48, Val-35, Leu-51, and Glu-52. In all spectra obtained, NOEs to the myristate were observed, but no new intraprotein NOEs were detected that would be indicative of an altered protein conformation. In addition, the relative NOE intensities and cross-peak patterns matched the data obtained for the WT myr(s)MA protein. [27,31]

The main differences between the structures are localized within the disordered loop formed by residues Gly-2 – Ser-9. For V7R, the side chain of Arg-7 is poised to make a salt bridge with the side chain of Glu-52, and the mythelene groups of Arg-7 contribute to the hydrophobic interactions with the methylene groups of the myristate (Figure 6). For L8A, the smaller size of Ala-8 creates a better cavity for the myristate group, which packs closer to Trp-16 as evidenced by the upfield shift of the terminal myr-$C^{14}H_3$ (Figure 6). Thus, structural changes implicated by the chemical shift data involve only residues located near the mutation site, which may have only average intrinsic conformational mobility.

PI(4,5)P_2 binds to myrMA mutants but does not trigger myristate exposure

Binding studies were conducted with di-C_4-phosphatidylinositol phosphate (di-C_4-PI(4,5)P_2), a soluble form of PI(4,5)P_2 containing truncated lipids. Representative ^{1}H-^{15}N HSQC NMR data obtained upon titration of V7R with di-C_4-PI(4,5)P_2 are shown in Figure 7. Titration of di-C_4-PI(4,5)P_2 led to significant changes in the backbone ^{1}H and ^{15}N NMR chemical shifts of residues Arg-22, Lys-26, Lys-27, His-33, Glu-73, Glu-74, Leu-75 and Ser-77, (Group 1; $\Delta\delta HN$ $((\Delta\delta 1_H)^2+(\Delta\delta 15_N)^2)^{1/2}$ = 0.1–0.8 ppm) (Figure 7). These residues reside on the β-II-V cleft, and were previously shown to contribute to the PI(4,5)P_2 binding site. Non-linear least squares fits of the titration data afforded a dissociation constant (K_d) value (261 ± 18 μM), similar to those observed for WT myr(-)MA and myrMA (Figure 7 and Table 2). Titration of di-C_4-PI(4,5)P_2 into L8A and L8I mutants also led to signal shifts and K_d values that are very similar to those obtained for V7R (Table 2). NMR data obtained for V7R (Figure 7), L8A, and L8I proteins confirmed that di-C_4-PI(4,5)P_2 binds to these mutants in a manner identical to that observed for the WT myr(-) and myrMA proteins [31].

Interestingly, ^{1}H and ^{15}N NMR signal corresponding to residues Gly-2-Ser-9, Glu-12-Asp-15, Arg-39, and His 89 “group 2” did not exhibit detectable chemical shift changes upon titration of V7R, L8A, and L8I with di-C_4-PI(4,5)P_2 (Figure 7). Chemical shift changes of “group 2” were observed for WT myrMA upon addition of di-C_4-PI(4,5)P_2 and NMR-based structural studies confirmed that they reflect di-C_4-PI(4,5)P_2-dependent exposure of the myristyl group.[31] In addition, intermolecular NOEs between protein residues and myristate group are clearly observed in the 3D ^{13}C-edited/^{12}C-double-half-filtered NOE experiment obtained for the V7R:di-C_4-PI(4,5)P_2 complex (Figure 7), indicating that di-C_4-PI(4,5)P_2 binding does not trigger myristyl exposure.

Compensatory mutant V7R/L21K-myrMA binds PI(4,5)P_2 with enhanced affinity

To understand how a compensatory mutation (Leu-21) reversed the membrane-binding defect imposed by V7R, we collected NMR and thermodynamic data for V7R/L21K and L21K protein samples. 2D [^{1}H–^{15}N] HSQC spectra obtained for L21K at concentrations of 50 – 900 μM showed that as protein concentration is increased, several signals (e.g., those corresponding to Ser 6, Gly 10, Gly 11) shifted progressively towards the corresponding frequencies of myr(-)MA. These signal shifts are similar to those observed for WT myrMA, and are indicative of a shift in equilibrium from myr(s) to myr(e) form. SE data obtained for L21K protein confirm that the protein exists in a monomer-trimer equilibrium with $K_{assoc} = 3.7 \pm 0.4 \times 10^8\ M^{-2}$ (data not shown). Interestingly, [^{1}H–^{15}N] HSQC spectra for V7R/L21K show that signals were insensitive to protein concentration and SE data confirm that V7R/L21K is a monomer, indicating that a second mutation (L21K) does not trigger myristyl exposure.

Structural studies on the WT myrMA protein bound to PI(4,5)P_2 revealed that the side chains of Leu-21 play a major role in stabilizing the hydrophobic interactions with the 2'-acyl chain of PI(4,5)P_2. Thus, we hypothesized that substitution of Leu-21 with lysine may affect the binding affinity of PI(4,5)P_2 to the MA protein. For L21K and V7R/L21K, ^{1}H-^{15}N HSQC NMR data obtained upon titration with di-C_4-PI(4,5)P_2 showed that "group 1" peaks exhibited similar shifts to those observed for V7R, L8A and L8I as well as WT myr(-)MA and myrMA. Non-linear least squares fits of the titration data for L21K and V7R/L21K afforded binding affinity values (Figure 7 and Table 2), which are ~2-fold greater than WT myrMA. For L21K, group 2 signals also exhibited di-C_4-PI(4,5)P_2-dependent 1H-15N HSQC signals that shift progressively toward values observed for myr(-)MA. Analysis of a combination of ^{15}N-, ^{15}N/^{13}C- and ^{13}C-edited/^{12}C-double-half-filtered NOE experiments confirm that di-C_4-PI(4,5)P_2 binds to the II-V-β cleft on L21K and V7R/L21K in a manner very similar to the WT myrMA protein (Figure 7). Interestingly, for V7R/L21K the ^{1}H-^{15}N HSQC signals corresponding to "group 2" residues did not exhibit chemical shift changes upon titration with di-C_4-PI(4,5)P_2, indicating that although di-C_4-PI(4,5)P_2 binds to V7R/L21K with affinity similar to that observed for L21K, that binding does not trigger myristate exposure.

Point mutations near the amino-terminus of myrMA inhibit PM binding *in vivo*

Previous studies demonstrated that point mutations near the amino terminus of myrMA can lead to defects in membrane association. [19,24–26] We have now determined the *in vivo* localization patterns of HIV-1 Gag proteins containing the following point mutations: L8E, L8V, S9A, S9E, V7R, and V7R/L21K (Figure 1). As expected from our membrane binding studies, all of the single mutants show an increase in hazy cytosolic staining relative to WT (Figure 8), consistent with their membrane-binding defect. This hazy, non-punctate staining pattern is typical of HIV-1 Gag mutants that are defective in membrane binding[33,34]. This Gag localization phenotype is distinct from that induced by mutations in the MA "80's domain" or the MA basic domain, which show retargeting to the MVB [5,12,19,35]. Thus, consistent with earlier biochemical data[24], these mutations appear to induce defects in membrane binding rather than targeting. Interestingly, V7R/L21K displays a highly punctate, non-diffuse cell-surface Gag localization pattern, consistent with the ability of the L21K mutation to correct the membrane-binding defect imposed by V7R[24].

Discussion

Previous *in vivo* mutagenesis studies have provided important insights into the mechanism of retrovirus assembly. Mutations of the first five residues of the HIV-1 MA domain that inhibit myristoylation lead to the accumulation of Gag in the cytosol, indicating that myristoylation is required for efficient membrane binding. Substitution of basic residues between Lys-18 and Lys-32, which form a basic patch on the surface of MA, retargets Gag to a cytoplasmic

compartment [5,12,19,35], and *in vitro* membrane binding studies support the hypothesis that the myristyl group and basic patch cooperatively facilitate membrane binding [5,12,19,35]. Mutations at positions 7 and 8 of the MA domain (V7R, L8A, and L8I), which do not inhibit myristoylation, have also been shown to inhibit membrane binding in cells, suggesting that the mutations might inhibit myristate exposure. [19,24–26] The findings presented here demonstrate that these mutations inhibit PM localization *in vivo* and turn off the myristyl switch. The myristyl switch equilibrium is sensitive to subtle molecular changes, and even the conservative substitution of Leu-8 by Ile is sufficient to block myristate exposure under conditions in which exposure is normally highly favored. These studies further demonstrate that the mutations lead to only minor structural changes that are proximal to the mutation sites.

Recent studies indicate that PI(4,5)P_2, a member of a family of differentially phosphorylated phosphatidylinositides that serve as membrane markers for specific cellular proteins [28–30], plays a critical role in the ultimate localization of Gag at the PM.[32] PI(4,5)P_2 is normally associated with the inner leaflet of the plasma membrane [29], and depletion of PI(4,5)P_2 leads to accumulation of Gag at the membranes of late endosomes and MVBs [32]. In addition, induction of PI(4,5)P_2-enriched endosomes retargets Gag to endosomes and induces intra-vesicle budding [32]. In both cases, virus production is severely attenuated[32]. PI(4,5)P_2 binds MA in an “extended lipid” conformation in which the inositol head group and the 2’-fatty acid chain bind to a hydrophobic cleft formed by helices II and V, and a meandering β-hairpin (β-II–V), and the remaining 1’-fatty acid and exposed myristyl group bracket a conserved basic surface patch previously implicated in membrane binding[36]. These findings suggested to us that the position-7 and –8 mutations, and the revertant mutants, might affect PI(4,5)P_2 binding or the sensitivity of PI(4,5)P_2 binding on the myristyl switch. The present studies demonstrate that PI(4,5)P_2 binds to V7R, L8A, and L8I with affinities similar to that observed for the native protein. Furthermore, the NMR chemical shift and NOE data indicate these mutants bind PI(4,5)P_2 in a manner that is essentially identical to that observed for the wild-type protein. However, PI(4,5)P_2 binding does not trigger myristate exposure in the V7R, L8A and L8I mutants, indicating that the coupling between the PI(4,5)P_2 binding site and the pocket that sequesters the myristyl group is weak. The fact that PI(4,5)P_2 binding is not attenuated by these mutations suggests that membrane binding *in vivo* may be mediated by a tripartite mechanism, in which the exposed myristyl group, the extended PI(4,5)P_2 bridge, and the basic patch collectively contribute to binding.

The defects in virus assembly and membrane binding imposed by amino acid substitutions at positions 7 and 8 can be reversed by intragenic second-site changes in the core of the protein[24–26]. In particular, L21K and K98E reversed the phenotype imposed by V7R, which led to the suggestion that these second mutations likely trigger myristate exposure to facilitate membrane binding. The present studies unexpectedly reveal that substitution of Leu-21 by Lys does not promote myristate exposure in either the L21K or L21K/V7R MA proteins. Instead, these mutants bind PI(4,5)P_2 with ~2-fold greater affinity than either the WT or V7R, L8A, and L8I mutants of the MA protein. It thus appears that this rather modest increase in binding affinity is sufficient to compensate for the inability of the protein to expose its myristyl group.

In related studies, the substitution of Val-7 and Leu-8 by glutamine (V7Q and L8Q) in the simian immunodeficiency virus (SIV) MA protein was shown to dramatically inhibit virus production and membrane association without affecting myristoylation [37]. HIV-1 and SIV MA proteins are highly homologous (~50% sequence identity and ~80% homologous), and the three-dimensional structures of the unmyristoylated MA proteins solved by NMR and X-ray techniques are very similar [36,38,39]. It is thus likely that the mechanism used by SIV to regulate membrane targeting and binding is similar to the mechanism employed by HIV-1.

In summary, we have demonstrated that mutations near the amino-terminus of the HIV-1 MA protein that inhibit membrane binding *in vitro* also lead to cytosolic localization of Gag *in vivo*. This loss of membrane association is due to the inability of the mutant MA proteins to expose their myristyl group. The myristyl switch equilibrium is highly sensitive to mutations near the N-terminus of the protein, and even the conservative substitution of Leu 8 by Ile is sufficient to "lock off" the myristyl switch. The myristyl switch unexpectedly remains locked off in the revertant mutant V7R/L21K, which assembles at the PM and exhibits a wild-type phenotype. This behavior appears to result from enhanced interactions with $PI(4,5)P_2$, which binds L21K- and V7R/L21K-MA with affinities that are about two-fold greater than that of the native MA protein. However, we cannot rule out the possibility that the increased charge and location of the L21K substitution might also directly influence membrane binding, and future studies of the interactions between these proteins with membranes, including those containing $PI(4,5)P_2$, are warranted.

Materials and Methods

Sample preparation

HIV-1 myrMA constructs containing amino acid changes V7R, L8I, L8A, L21K and V7R/L21K were made by using QuickChange XL site-directed mutagenesis kit (Stratagene, La Jolla, CA) and sequenced at the DNA sequencing facility, UMBC. Protein samples were prepared as described,[27,38] except that a modified protocol was applied to prepare ^{15}N-, and ^{13}C-,^{15}N-labeled samples.[40] Cells were first grown in 4L LB media at 37°C until $O.D._{600}$ reached ~0.6 – 0.7. Next, cells were spun down and washed with 1X M9 salt before transferring them to 1L M9 minimal media containing $^{15}NH_4Cl$ as the sole nitrogen source to produce 15N-labeled protein. At this stage, cells were supplemented with myristic acid (10 mg/liter; Sigma) then were grown for 1h before induction with isopropyl -D-thiogalactoside (1 mM). Cells were grown at 37°C for ~12 – 14h, lysed using microfluidizer, and the proteins purified by cobalt affinity chromatography (Clontech, Mountain View, CA) and ion exchange column chromatography (SP column). Traces of unmyristoylated species (for L21K) were separated from myristoylated sample by butyl-Sepharose hydrophobicity chromatography (GE Healthcare, Pittsburg, PA). We obtained a high yield (~25 mg/L) of 93 – 97% isotopically ^{15}N- and $^{15}N/^{13}C$-enriched proteins. Molecular weights and efficiency of myristylation were confirmed by electrospray ionization mass spectrometry. Phosphoinositide di-C_4-$PI(4,5)P_2$ (Echelon, Salt Lake City, UT) was obtained commercially and used without further purification. Samples for all NMR experiments were prepared in 50 mM sodium phosphate at pH 5.5, 100 mM NaCl and 5 mM DTT. NaCl was excluded from the NMR buffer for di-C_4-$PI(4,5)P_2$ titration experiments.

NMR spectroscopy

NMR data were collected with Bruker DRX (800 MHz ^1H) and DMX (600 MHz ^1H) spectrometers equipped with cryoprobes, processed with NMRPIPE[41] and analyzed with NMRVIEW[42]. A combination of two-, three- and four-dimensional NOESY data were obtained for combinations of natural abundance, ^{15}N- and ^{15}N-,^{13}C-labeled protein samples (35 °C). Protein backbone signals were assigned using standard triple resonance methods (HNCA and HNCOCA), and side chain signals were assigned from 3D and 4D ^{15}N-, ^{13}C-, and $^{15}N/^{13}C$-edited NOESY data. Intermolecular ^1H-^1H NOEs between ^{15}N-,^{13}C-labeled protein and unlabeled myristate group were assigned from 2D (^1H-^1H) and 3D (^{13}C- and ^{13}C-edited/^{12}C-double-half-filtered) NOESY data (see references [43–45] and citations therein). ^1H-^{15}N residual dipolar couplings were measured using a modified in-phase/anti-phase (IPAP) HSQC experiment [46] for V7R and L8A samples aligned in polyacrylamide gel [47]. Binding isotherms from ^1H-^{15}N NMR HSQC titration experiments were calculated with ORIGIN 7.0 software (MicoCal, Northampton, MA).

Analytical ultracentrifugation

Sedimentation equilibrium measurements were collected on a Beckman XL-I Optima system equipped with a four-hole An-60 rotor (Beckman Coulter) and cells were equipped with double-sectored centerpieces of path length 12 or 3 mm and quartz windows. Protein samples were prepared in 50 mM sodium phosphate buffer at pH 5.5 containing 100 mM NaCl and 2 mM Tris (2-carboxy-ethyl)-phosphine-HCl. Loading concentrations varied from 50 to 150 μM for all samples. Rotor speeds were at 22,000 and 26,000 rpm, and temperature was 20 °C. Scans were obtained by using the absorption optics system with 0.002 cm step size and four averages per point, and acquired at wavelengths of 280 and 295 nm. Partial specific volumes (v-bar) and molar extinction coefficients were calculated by using the program SEDNTERP (www.jphilo.mail-way.com) and buffer densities were measured pycnometrically. Data analysis was performed by using NONLIN.[48] Equilibrium association constants were determined by global analysis of data acquired from samples prepared at two loading concentrations and centrifuged at two rotor speeds.

Structure calculations

Structures were calculated in torsion angle space with CYANA (http://www.las.jp/index_eg.html) starting from random initial angles. Upper interproton distance bounds of 2.7, 3.3 and 5.0 Å (with appropriate corrections for pseudoatoms) were employed for NOE cross peaks of strong, medium, and weak intensity respectively, which were qualitatively determined following intensity normalization of the different NOE data sets. No backbone hydrogen bond or chemical shift-based torsion angle restraints were employed. Statistical information is provided in Table 1. Structure figures were generated with PyMOL (http://pymol.sourceforge.net).

Fluorescence microscopy

Construction of derivatives of the HIV-1 pNL4-3 clone containing MA mutations V7R, L8V, L8E, S9A, S9E and V7R/L21K has been described elsewhere.[19,24,25] The numbering scheme of these mutations has been changed to be consistent with the scheme we used in earlier structural studies. HeLa cells cultured in chamber slides (Nunc) were transfected with either wild type pNL4-3 or the indicated MA mutants in the pNL4-3 backbone using the Lipofectamine 2000 reagent (Invitrogen, Carlsbad, CA). Cells were fixed 24–48 hr posttransfection with 3.7% formaldehyde in 100 mM sodium phosphate buffer (pH 7.2) for 20 min, and permeabilized with phosphate-buffered saline (PBS) containing 0.1% Triton X-100. Gag protein in transfected cells was visualized by incubating with anti-p17 monoclonal antibody (Advanced Biotechnologioes Inc, Columbia, MD) diluted in PBS containing 3% BSA followed by Texas red-conjugated anti-mouse IgG. Cells were mounted with Aqua Poly Mount (Polysciences Inc, Warrington, PA) and examined using a Delta Vision RT microscope.

Atomic coordinates

The atomic coordinates have been deposited in the Protein Data Bank, www.pdb.org, and are available under the accession codes 2JMG and 2NV3 for V7R and L8A, respectively.

Supplementary Material

Refer to Web version on PubMed Central for supplementary material.

Acknowledgements

This work was supported by NIH grant AI30917. We thank the HHMI staff and colleagues at UMBC, Dr. Dorothy Beckett (University of Maryland, College Park), and David King (HHMI, U.C. Berkeley) for technical support. This research was supported in part by the Intramural Research Program of the NIH, National Cancer Institute, Center for

Cancer Research (EOF). P.J. and M.L. are Meyerhoff undergraduate scholars, and E.L. and J.T. are UMBC Presidential and MARC undergraduate scholars, respectively.

References

1. Coffin, JM.; Hughes, SH.; Varmus, HE. Retroviruses. Cold Spring Harbor Laboratory Press; Plainview, N.Y.: 1997.
2. Morita E, Sundquist WI. Retrovirus Budding. Annual Review of Cell and Develpomental Biology 2004;20:395–425.
3. von Schwedler UK, Stuchell M, Muller B, Ward DM, Chung HY, Morita E, Wang HE, Davis T, He GP, Cimbora DM, Scott A, Krausslich HG, Kaplan J, Morham SG, Sundquist WI. The protein network of HIV budding. Cell 2003;114:701–713. [PubMed: 14505570]
4. Dong X, Li H, Derdowski A, Ding L, Burnett A, Chen X, Peters TR, Dermody TS, Woodruff E, Wang JJ, Spearman P. AP-3 directs the intracellular trafficking of HIV-1 Gag and plays a key role in particle assembly. Cell 2005;120:663–674. [PubMed: 15766529]
5. Hermida-Matsumoto L, Resh MD. Localization of Human Immunodeficiency virus Type 1 Gag and env at the Plasma Membrane by Confocal Imagine. Journal of Virology 2000;74:8670–8679. [PubMed: 10954568]
6. Nguyen DG, Booth A, Gould SJ, Hildreth JE. Evidence that HIV budding in primary macrophages occurs through the exosome release pathway. J Biol Chem 2003;278:52347–52354. [PubMed: 14561735]
7. Ono A, Freed EO. Cell-Type-Dependent Tageting of Human Immunodeficiency Virus Type 1 Assembly to the Plasma Membrane and the Multivesicular body. Journal of Virology 2004;78:1552–1563. [PubMed: 14722309]
8. Raposo G, Moore M, Innes D, Leijendekker R, Leigh-Brown A, Benaroch P, Geuze H. Human macrophages accumulate HIV-1 particles in MHC II compartments. Traffic 2002;3:718–729. [PubMed: 12230470]
9. Jouvenet, N.; Neil, SJD.; Bess, C.; Johnson, MC.; Virgen, CA.; Simon, SM.; Bieniasz, PD. PLoS Biology. 2006. Plasma membrane is the site of productive HIV-1 particle assembly. in press
10. Ono A, Freed EO. Plasma membrane rafts play a critical role in HIV-1 assembly and release. Proc Natl Acad Sci USA 2001;98:13925–13930. [PubMed: 11717449]
11. Ono A, Freed EO. Role of lipid rafts in virus replication. Adv Virus Res 2005;64:311–358. [PubMed: 16139599]
12. Yuan X, Yu X, Lee TH, Essex M. Mutations in the N-Terminal Region of Human Immunodeficiency Virus Type I Matrix Protein Block Intracellular Transport of the Gag Precursor. Journal of Virology 1993;67:6387–6394. [PubMed: 8411340]
13. Zhou W, Parent LJ, Wills JW, Resh MD. Identification of a Membrane-Binding Domain Within the Amino-Terminal Region of Human Immunodeficiency Virus Type 1 Gag Protein Which Interacts with Acidic Phospholipids. Journal of Virology 1994;68:2556–2569. [PubMed: 8139035]
14. Bryant M, Ratner L. Myristoylation-Dependent Replication and Assembly of Human Immunodeficiency Virus 1. Proceedings of the National Academy of Sciences USA 1990;87:523–527.
15. Copeland NG, Jenkins NA, Nexo B, Schultz AM, Rein A, Mikkelsen T, Jorgensen P. Poorly expressed endogenous ecotropic provirus of DBA/2 mice encodes a mutant Pr65gag protein that is not myristylated. J Virol 1988;62:479–487. [PubMed: 2826810]
16. Göttlinger HG, Sodroski JG, Haseltine WA. Role of capsid precursor processing and myristoylation in morphogenesis and infectivity of human immunodeficiency virus type 1. Proceedings of the National Academy of Sciences USA 1989;86 :5781–5785.
17. Spearman P, Horton R, Ratner L, Kuli-Zade I. Membrane binding of human immunodeficiency virus type 1 matrix protein in vivo supports a conformational myristyl switch mechanism. J Virol 1997;71:6582–6592. [PubMed: 9261380]
18. Spearman P, Wang JJ, Vander Heyden N, Ratner L. Identification of Human Immunodeficiency Virus Type 1 Gag Protein Domains Essential to Membrane Binding and Particle Assembly. Journal of Virology 1994;68:3232–3242. [PubMed: 8151785]

19. Freed EO, Orenstein JM, Buckler-White AJ, Martin MA. Single Amino Acid Changes in the Human Immunodeficiency Virus Type 1 Matrix Protein Block Virus Particle Production. Journal of Virology 1994;68:5311–5320. [PubMed: 8035531]
20. Ono A, Orenstein JM, Freed EO. Role of the Gag Matrix Domain in Targeting Human Immunodeficiency Virus Type 1 assembly. Journal of Virology 2000;74:2855–2866. [PubMed: 10684302]
21. Bouamr F, Scarlata S, Carter CA. Role of myristylation in HIV-1 Gag assembly. Biochemistry 2003;42:6408–6417. [PubMed: 12767222]
22. Zhou W, Resh MD. Differential membrane binding of the human immunodeficiency virus type 1 matrix protein. J Virol 1996;70:8540–8548. [PubMed: 8970978]
23. Lindwasser OW, Resh MD. Myristoylation as a target for inhibiting HIV assembly: Unsaturated fatty acids block viral budding. Proc Natl Acad Sci USA 2002;99:13037–13042. [PubMed: 12244217]
24. Ono A, Freed EO. Binding of Human Immunodeficiency Virus Type 1 gag to membrane: Role of the matrix amino terminus. J Virol 1999;73:4136–4144. [PubMed: 10196310]
25. Ono A, Huang M, Freed EO. Characterization of human immunodeficiency virus type 1 matrix revertants: effects on virus assembly, Gag processing, and Env incorporation into virions. J Virol 1997;71:4409–4418. [PubMed: 9151831]
26. Paillart JC, Gottlinger HG. Opposing effects of human immunodeficiency virus type 1 matrix mutations support a myristyl switch model of Gag membrane targeting. J Virol 1999;73:2604–2612. [PubMed: 10074105]
27. Tang C, Loeliger E, Luncsford P, Kinde I, Beckett D, Summers MF. Entropic switch regulates myristate exposure in the HIV-1 matrix protein. Proc Natl Acad Sci USA 2004;101:517–522. [PubMed: 14699046]
28. Martin TFJ. PI(4,5)P2 regulation of surface membrane traffic. Curr Opin Cell Biol 2001;13:493–499. [PubMed: 11454457]
29. Behnia R, Munro S. Organelle identity and the signposts for membrane traffic. Nature 2005;438:597–604. [PubMed: 16319879]
30. McLaughlin S, Murray D. Plasma membrane phosphoinositide organization by protein electrostatics. Nature 2005;438:605–611. [PubMed: 16319880]
31. Saad JS, Miller J, Tai J, Kim A, Ghanam RH, Summers MF. Structural basis for targeting HIV-1 Gag proteins to the plasma membrane for virus assembly. Proc Natl Acad Sci USA 2006;103:11364–11369. [PubMed: 16840558]
32. Ono A, Ablan SD, Lockett SJ, Nagashima K, Freed EO. Phosphatidylinositol (4,5) bisphosphate regulates HIV-1 Gag targeting to the plasma membrane. Proceedings of the National Academy of Sciences 2004;101:14889–14894.
33. Joshi A, Nagashima K, Freed EO. Mutation of dileucine-like motifs in the human immunodeficiency virus type 1 capsid disrupts virus assembly, gag-gag interactions, gag-membrane binding, and virion maturation. Journal of Virology 2006;80:7939–7951. [PubMed: 16873251]
34. Ono A, Demirov D, Freed EO. Relationship between human immunodeficiency virus Type-1 Gag multimerization and membrane binding. J Virol 2000;74:5142–5150. [PubMed: 10799589]
35. Freed EO, Englund G, Martin AM. Role of the Basic Domain of Human Immondeficiency Virus Type 1 Matrix in Macrophage Infection. Journal of Virology 1995;69:3949–3954. [PubMed: 7745752]
36. Hill CP, Worthylake D, Bancroft DP, Christensen AM, Sundquist WI. Crystal Structures of the Trimeric HIV-1 Matrix Protein: Implications for Membrane Association. Proceedings of the National Academy of Sciences USA 1996;93:3099–3104.
37. Gonzalez SA, Affranchino JL. Substitution of Leucine 8 in Simian Immunodeficiency Virus Matrix Protein Impairs Particle Formation Without Affecting N-Myristylation of the Gag Precursor. Virology 1998;240:27–35. [PubMed: 9448686]
38. Massiah MA, Starich MR, Paschall C, Summers MF, Christensen AM, Sundquist WI. Three dimensional structure of the human immunodeficiency virus type 1 matrix protein. J Mol Biol 1994;244:198–223. [PubMed: 7966331]
39. Rao Z, Belyaev AS, Fry E, Roy P, Jones IM, Stuart DI. Crystal structure of SIV matrix antigen and implications for virus assembly. Nature 1995;378:743–747. [PubMed: 7501025]

40. Marley J, Lu M, Bracken C. A method for efficient isotopic labeling of recombinant proteins. Journal of Biomolecular NMR 2001;20:71–75. [PubMed: 11430757]

41. Delaglio F, Grzesiek S, Vuister GW, Zhu G, Pfeifer J, Bax A. NMRPipe: A multidimensional spectral processing system based on UNIX pipes. J Biomol NMR 1995;6:277–293. [PubMed: 8520220]

42. Johnson BA, Blevins RA. NMRview: a Computer Program for the Visualization and Analysis of NMR Data. J Biomol NMR 1994;4:603–614.

43. Wüthrich, K. NMR of Proteins and Nucleic Acids. John Wiley & Sons; New York: 1986.

44. Kay LE, Clore GM, Bax A, Gronenborn AM. Four-dimensional heteronuclear triple-resonance NMR spectroscopy of interleukin-1β in solution. Science 1990;249:411–414. [PubMed: 2377896]

45. Folkers PJM, Folmer RHA, Konings RNH, Hilbers CW. Overcoming the ambiguity problem encountered in the analysis of nuclear Overhauser magnetic resonance spectra of symmetric dimer proteins. J Am Chem Soc 1993;115:3798–3799.

46. Ishii Y, Markus MA, Tycko R. Controlling residual dipolar couplings in high-resolution NMR of proteins by strain induced alignment in a gel. J Biomol NMR 2001;21:141–151. [PubMed: 11727977]

47. Chou JJ, Gaemers S, Howder B, Louis JM, Bax A. A simple apparatus for generating streched polyacrylamide gels, yeilding uniform alignment of proteins and detergent micelles. J Biomol NMR 2001;21:377–382. [PubMed: 11824758]

48. Johnson ML, Faunt LM. Parameter estimation by least-squares methods. Methods Enzymol 1992;210:1–37. [PubMed: 1584035]

Abbreviations used

MA
: myristoylated HIV-1 matrix protein

Gag
: myristoylated HIV-1 Gag polyprotein

myr(-)
: unmyristoylated

myr(s)
: myristate-sequestered state

myr(e)
: myristate-exposed state

PI(4,5)P_2
: phosphatidylinositol-(4,5)-bisphosphate

NMR
: nuclear magnetic resonance

HSQC
: heteronuclear single quantum coherence

AU
: analytical ultracentrifugation

RDC
: residual dipolar coupling

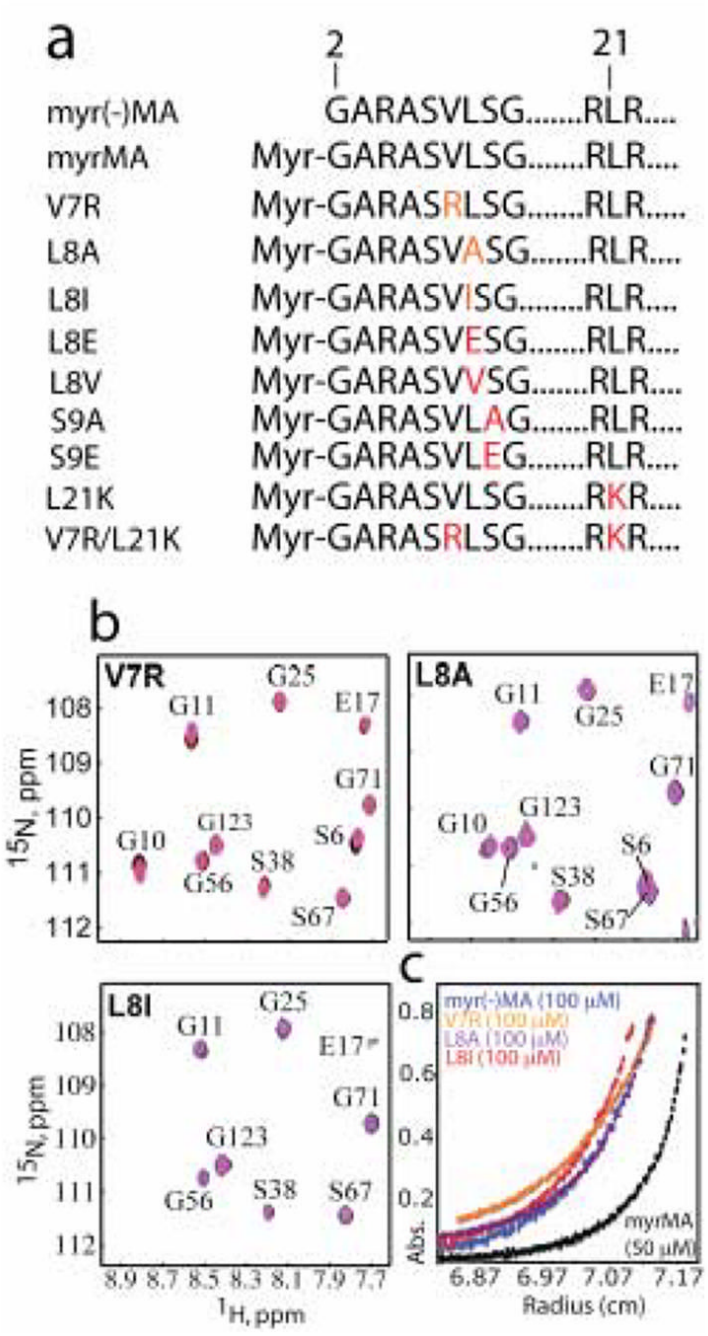

Figure 1.

(a) A representation of the MA sequence showing positions of the mutations in red. (b) Overlay of 2D ^{1}H-^{15}N HSQC spectra collected at different concentrations [600–900 μM (black), 300 μM red, 150 μM (blue), 50 μM (magenta)] for V7R, L8A, and L8I samples. (c) Representative sedimentation profiles obtained for myr(-)MA, WT and mutant myrMA proteins [(26,000 rpm, 20°C, 100 μM)]. For WT myrMA, best fits were obtained for a monomer-trimer equilibrium affording association constant (K_{assoc}) of $2.5 \pm 0.6 \times 10^{8}$ $M^{-2.27}$ Sedimentation equilibrium curves for myr(-)MA, V7R, L8A, and L8I fit best to monomeric species.

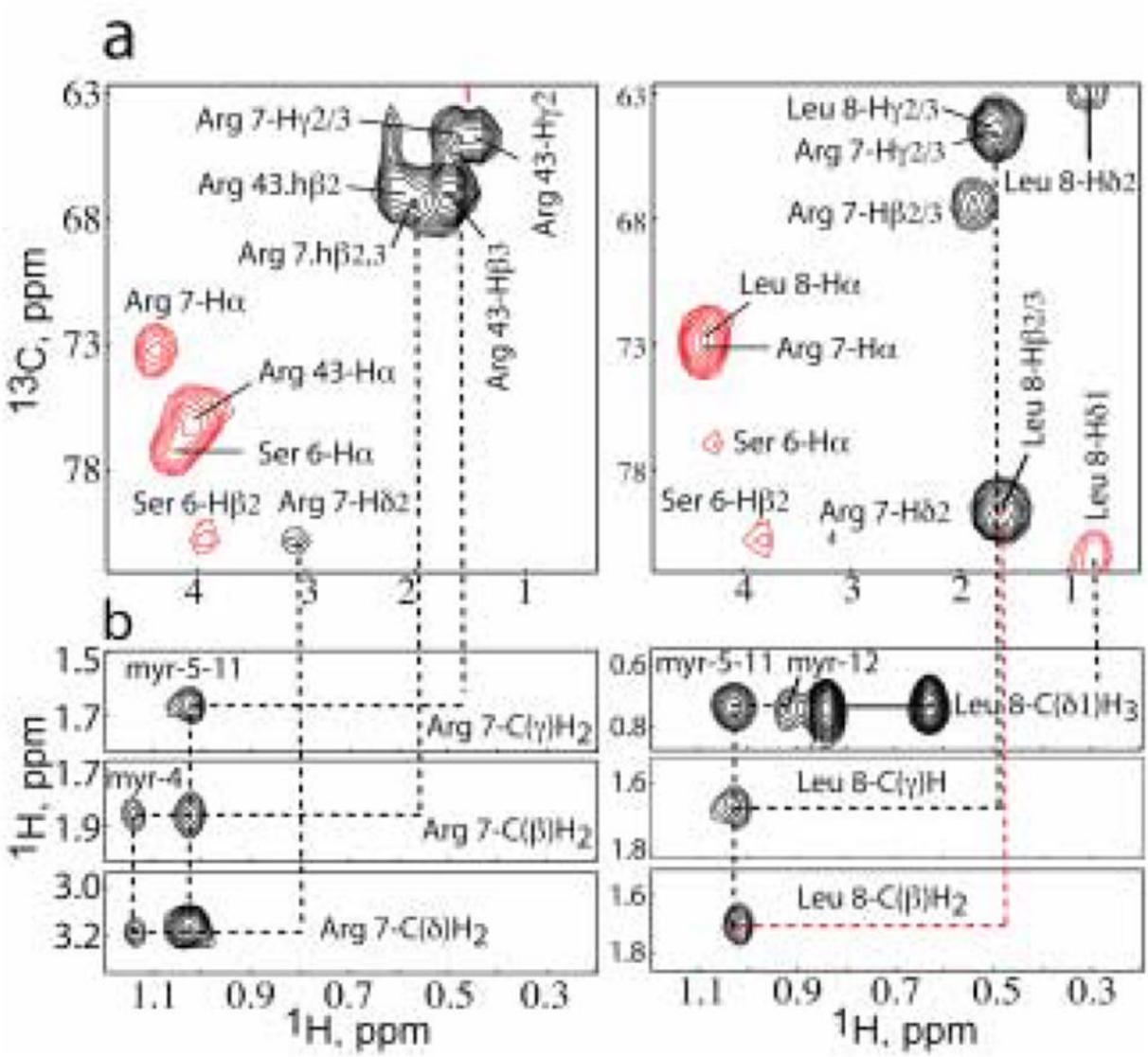

Figure 2.

Representative NMR data obtained for V7R. (a) 4D $^{15}N,^{13}C$-edited NOE data showing intramolecular and intermolecular NOEs for residues Arg-7 (left) and Leu-8 (right). NOE cross-peaks to the myristate group are not observed because the myristate group is not ^{13}C-labeled. (b) ^{13}C-edited/^{12}C-double-half-filtered NOE data showing unambiguously assigned intermolecular NOEs between unlabeled myristyl group and ^{13}C-labeled protein. Solid lines denote ^{1}H-^{12}C breakthrough doublets NOE peaks.

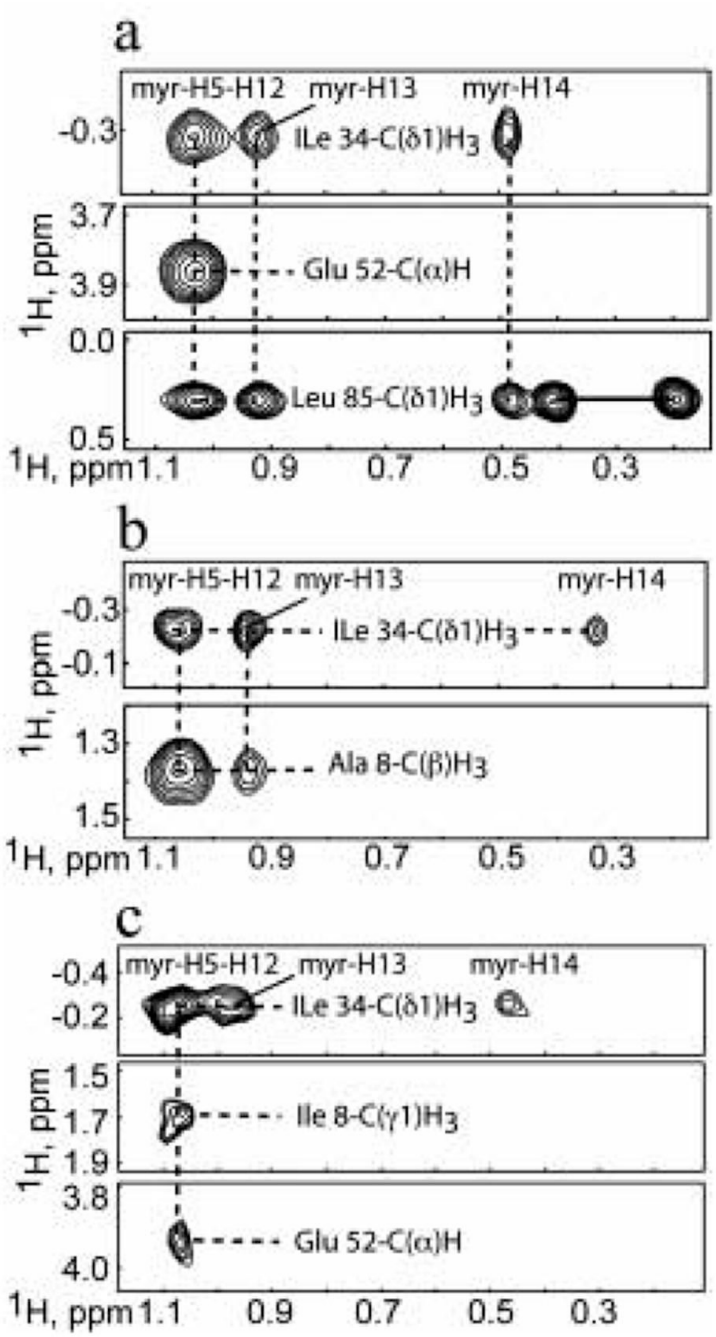

Figure 3.

(a) Representative ^{13}C-edited/^{12}C-double-half-filtered NOE data showing unambiguously assigned intermolecular NOEs between unlabeled myristyl group and ^{13}C-labeled V7R (a), L8A (b), and L8I (c). Solid and dashed lines denote ^{1}H-^{12}C breakthrough doublets and intermolecular NOE peaks, respectively.

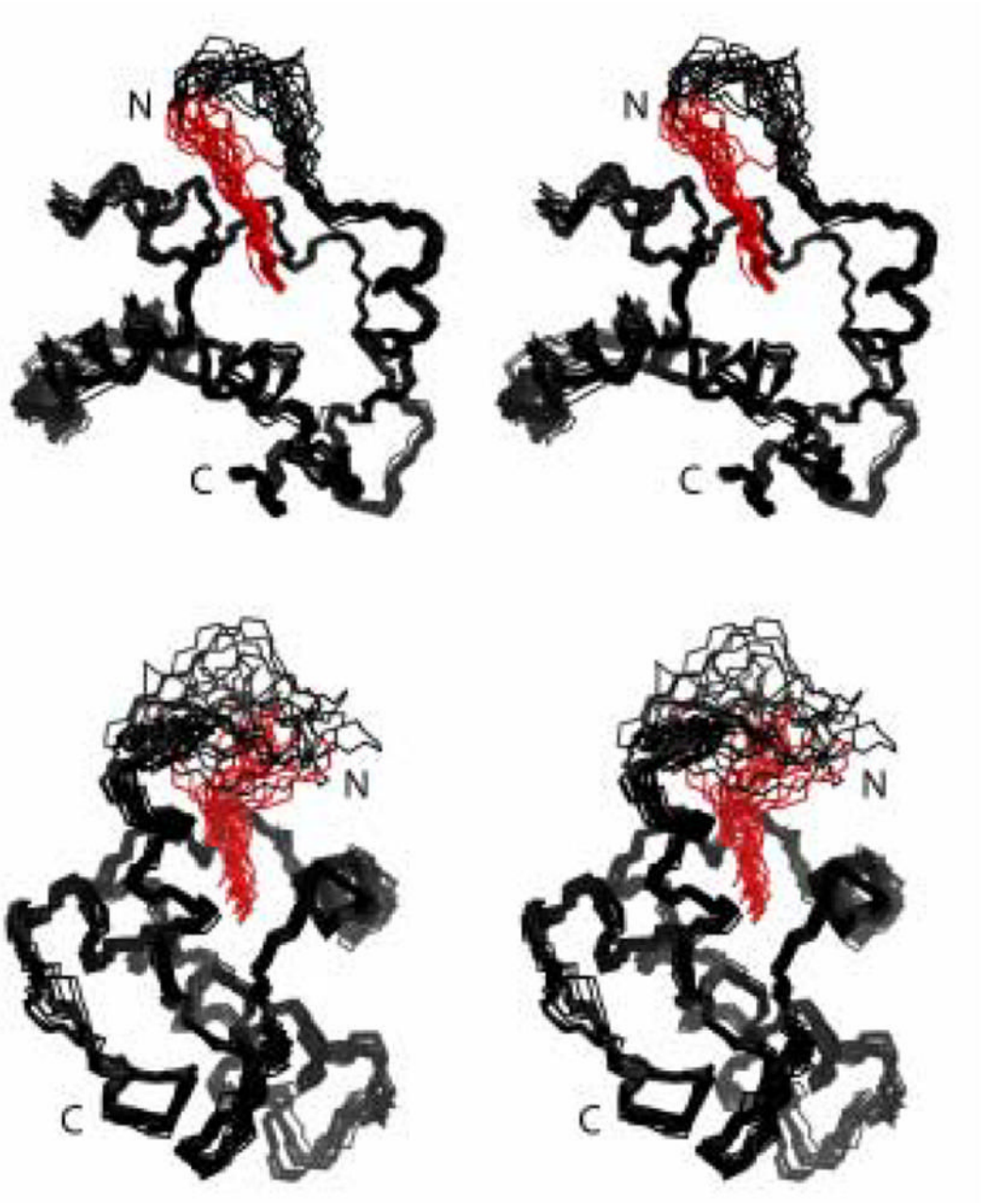

Figure 4.
Stereoviews showing the best-fit backbone superpositions of the 20 refined structures calculated for V7R (top) and L8A (bottom) proteins. Myristate group is shown in red.

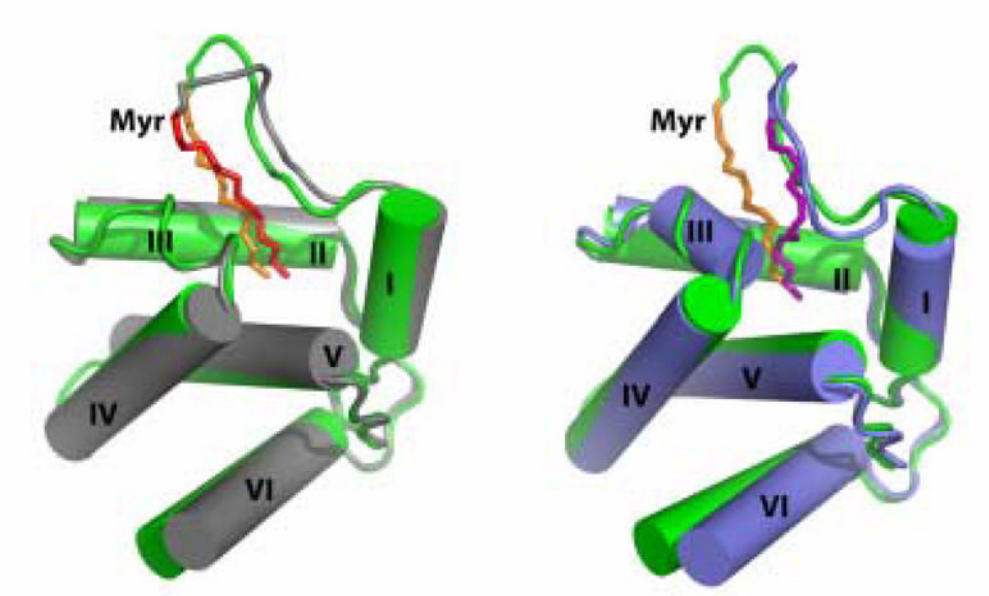

Figure 5.
Representative structures of V7R (grey) and L8A (slate) superimposed with WT myrMA protein (green). Myristate groups of WT myrMA, V7R- and L8A proteins are shown in orange, red and purple, respectively. NMR data revealed that Helix VI is flexible for native and mutant myrMA proteins.

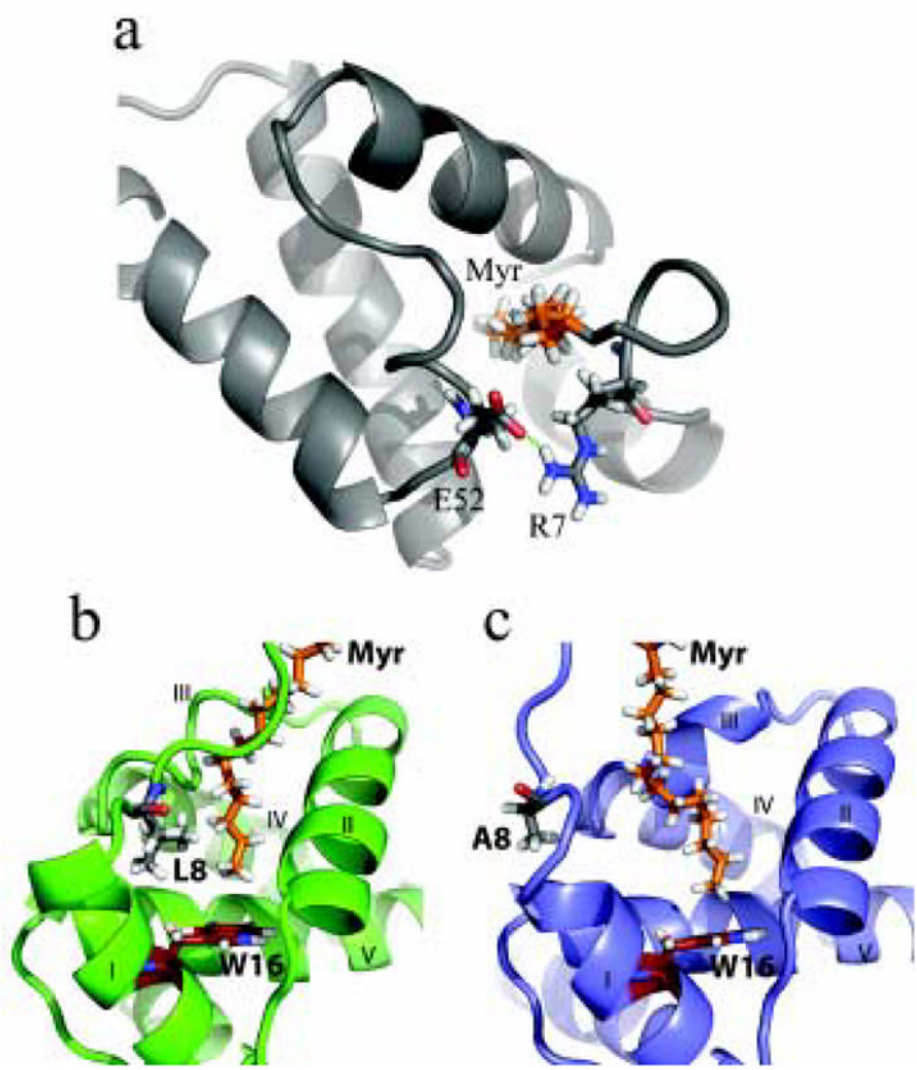

Figure 6.

Cartoon and stick representation showing minor conformational adjustments in the N terminus of V7R and L8A proteins compared with WT myrMA. (a) For V7R, a salt bridge between Arg-7 and Glu-52 stabilizes the myr(s) form. (b) When compared with WT myrMA (green), substitution of Leu-8 with Ala (slate, c) creates a better cavity for the myristate group (orange) and allows for the terminal methyl of myristate group to pack closer to Trp-16 (firebrick).

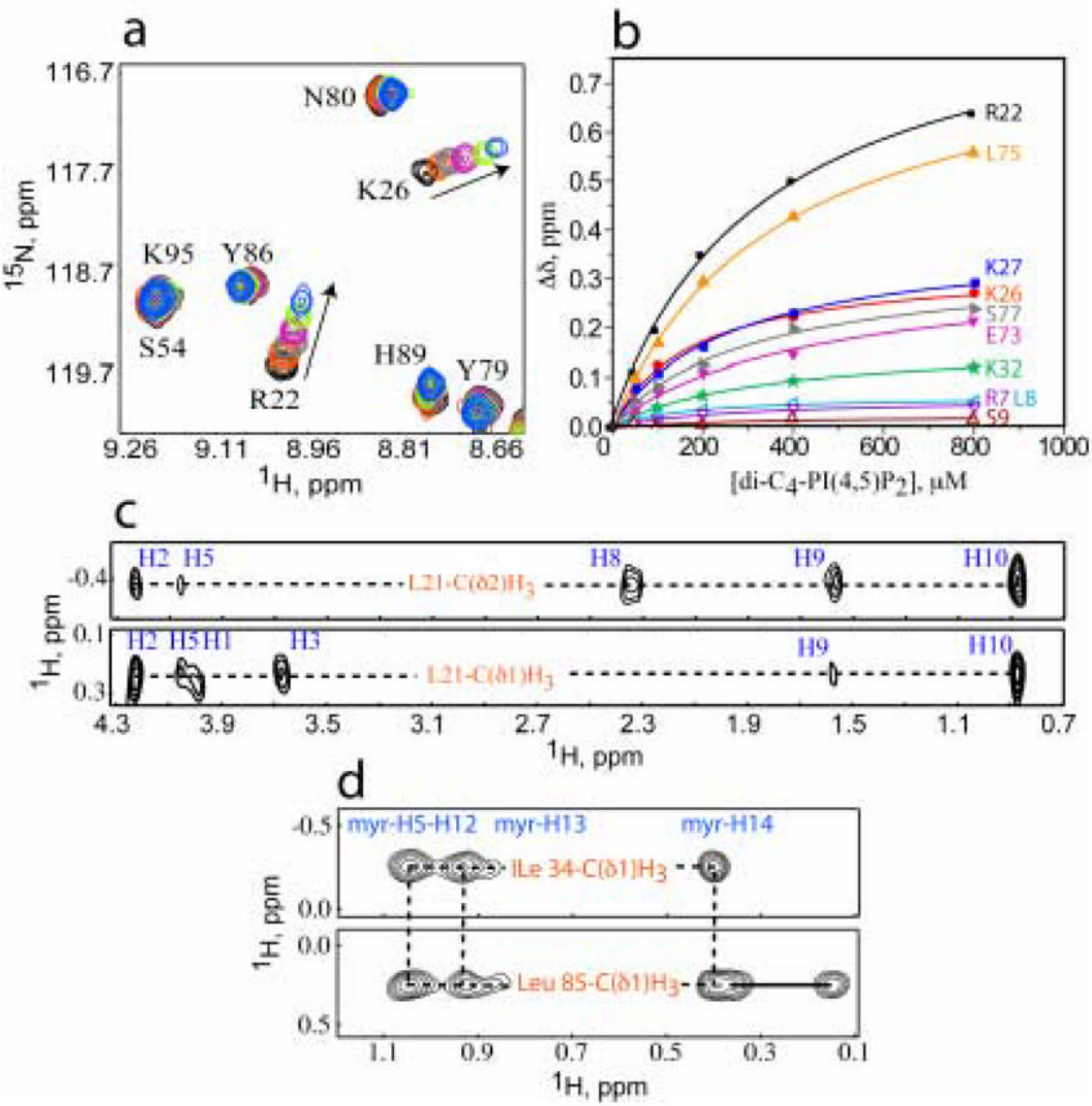

Figure 7.

(a) Overlay of 2D ^{1}H-^{15}N HSQC spectra upon titration of V7R with di-C$_4$-PI(4,5)P$_2$ [50 μM, 35 °C; di-C$_4$-PI(4,5)P$_2$:MA = 0:1 (black), 1:1 (red) , 2:1 (grey), 4:1 (magenta), 8:1 (green), 16:1 (blue)]. (b) ^{15}N NMR chemical shift titration data, which fit to 1:1 binding isotherms (K_d = 261 ± 18 μM). Representative ^{13}C-edited/^{12}C-double-half-filtered NOE data showing unambiguously assigned intermolecular NOEs between (c) Leu-21 and di-C$_4$-PI(4,5)P$_2$, and (d) Ile-34 and Leu-85 to the myristate group. Solid and dashed lines denote ^{1}H-^{12}C breakthrough doublets and intermolecular NOE peaks, respectively.

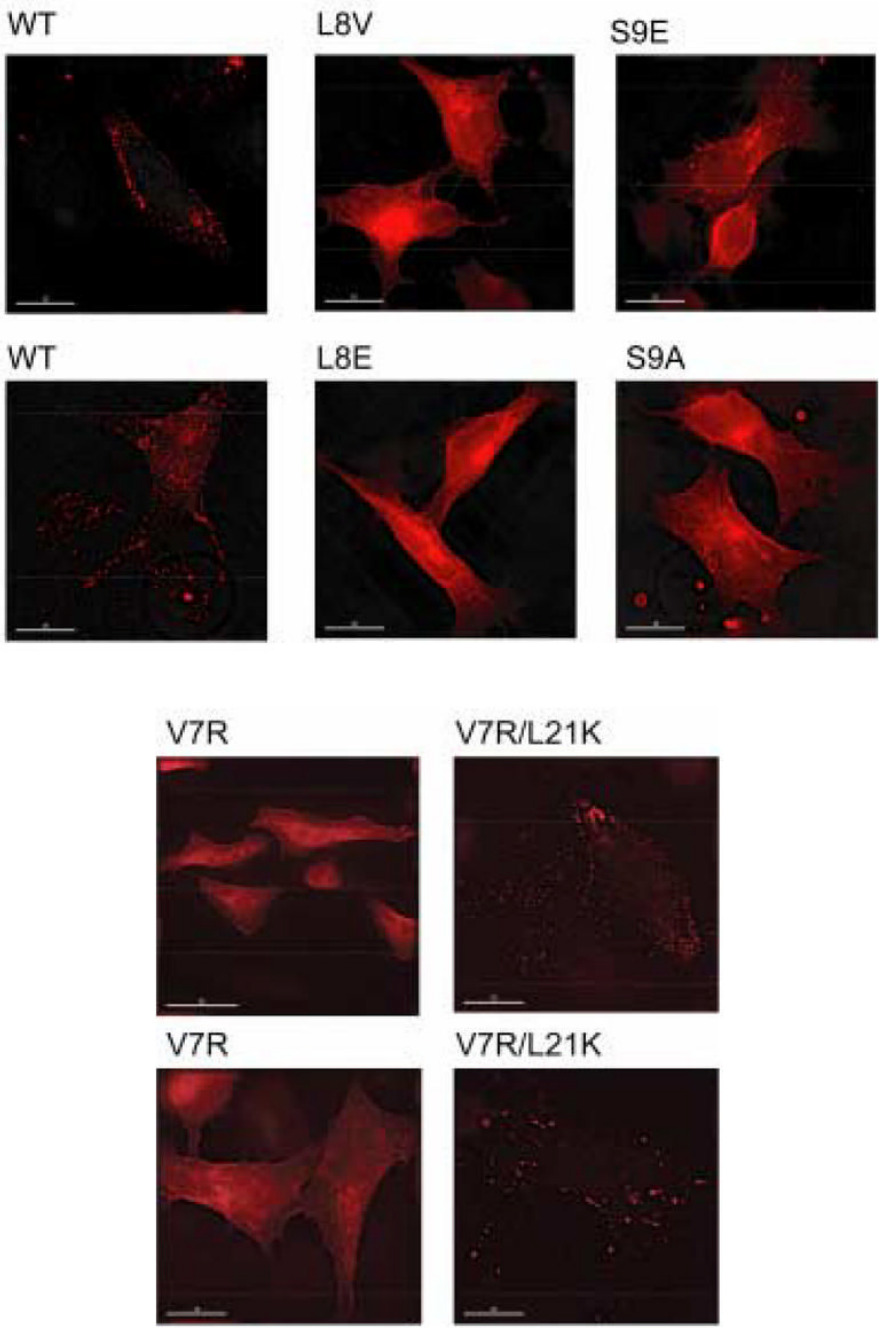

Figure 8.
Subcellular localization of MA mutants. HeLa cells were transfected with WT pNL4-3 or derivatives encoding the indicated MA mutants. Cells were fixed, permeabilized, and stained with anti-p17 monoclonal antibody and Texas red-conjugated anti-mouse IgG. Cells were mounted and examined using a Delta Vision RT microscope and the images were deconvolved. Two representative fields for WT, V7R, and V7R/L21K are shown.

Table 1

Statistics for HIV-1 V7R and L8A-myrMA Structures[1]

NMR-derived restraints	V7R	L8A
^{1}H-^{13}H distance restraints	834	818
Intraresidue	81	80
Sequential(| i − j| = 1)	165	166
Medium & Long range(| i − j | > 1)	579	565
Backbone H-bonds (4/H-bond)	0	0
Side-chain H-bonds (4/H-bond)	20	16
Dipolar coupling restraints	87	88
Intermolecular	0	0
Average restraints/refined residue	14.8	14.1
Target function (Å^2)		
Mean (± Std Dev)	1.29 (0.23)	1.56 (0.20)
Minimum	0.79	0.98
Maximum	1.58	1.73
Restraint violations		
Av. max. upper dist. viol. (Å)	0.36	0.39
(± Std Dev)	0.06	0.09
Av. max. VDW viol. (Å)	0.30	0.28
(± Std Dev)	0.07	0.08
Av. max RDC viol. (Hz)	0.40	0.36
(± Std Dev)	0.16	0.11
Structure Convergence (Å)[2]		
Main chain atoms		
Mean (± Std Dev)	0.48 (0.11)	0.58 (0.08)
All heavy atoms		
Mean (± Std Dev)	0.95 (0.10)	1.02 (0.09)

[1] A total of 20 refined structures per ensemble (see Materials and Methods for structure refinement details).

[2] RMSDs calculated relative to mean atom coordinates for residues 10 to 30 and 35 to 100

Table 2

Summary of K_d (μM) values for di-C_4-PI(4,5)P_2 binding to MA proteins.

Sample	Kd (μM)
myr(-)MA[a]	240 ± 60
myrMA[a]	150 ± 30
V7R	261 ± 18
L8A	150 ± 24
L8I	108 ± 5
L21K	67 ± 5
V7R-L21K	84 ± 9

[a]Values reported previously (ref 31)